PCCP

Accepted Manuscript

ROYAL SOCIETY OF CHEMISTRY

www.rsc.org/pccp

Journal Name

RSCPublishing

ARTICLE

Structural effect on the photophysical properties of mono-β-diketonate and bis-β-diketonate Eu^{III} complexes

Tianyu Zhu, Peng Chen, Hongfeng Li,* Wenbin Sun, Ting Gao, Pengfei Yan*

Cite this: DOI: 10.1039/x0xx00000x

Received 00th January 2012,
Accepted 00th January 2012

DOI: 10.1039/x0xx00000x

www.rsc.org/

Two chemical structure similar ligands, mono-β-diketone (p-methoxylbenzoyl)trifluoroacetone (MBTF) and bis-β-diketone 1,2-bis(4,4'-bis(4,4,4-trifluoro-1,3-dioxobutyl))phenoxyl ethane (BTPE) have been designed and prepared for the purpose of building the relationships between the structures and luminescence properties of Eu(III) complexes. Structures of their Eu(III) complexes $[Eu(MBTF)_3(DMSO)(H_2O)]$ and $[Eu_2(BTPE)_3(DMSO)_4]$ have been defined by single crystal X-ray crystallography. The mono-β-diketone complex $[Eu(MBTF)_3(DMSO)(H_2O)]$ is a mononuclear structure, the central Eu(III) ion is coordinated by eight oxygen atoms from three ligands and two solvents, in an distorted trigonal-dodecahedral (8-TDH) geometry. Whereas, the bis-β-diketone complex $[Eu_2(BTPE)_3(DMSO)_4]$ adopts triple-stranded dinuclear structure in which the two Eu(III) are helically wrapped by three bis-bidentate ligands, and each Eu(III) ion is eight-coordinated by six oxygen atoms from the ligands and two oxygen atoms from the coordinated DMSO molecules, in a distorted square-antiprismatic (8-SAP) geometry. The photophysical properties related to the electronic transition are characterized by the absorbance spectra, the emission spectra, the emission quantum yields, the emission lifetimes, and the radiative (k_r) and nonradiative rate constants (k_{nr}). The mono-β-diketone complex $[Eu(MBTF)_3(DMSO)(H_2O)]$ offers a relatively high emission quantum yield (38%, in solid) compared to that observed in the bis-β-diketone complex $[Eu_2(BTPE)_3(DMSO)_4]$ (25%, in solid). This enhancement of emission quantum yield in mono-β-diketone complex can be attributed to its lower site symmetry around the Eu(III) ion, lower non-radiative rate constant and higher energy transfer efficiency from ligand to metal ion.

Introduction

Luminescent lanthanide complexes have received a great deal of attentions over the last two decades because of their wide range of photonic applications such as tunable lasers, light emitting diodes, optical amplifiers, luminescence probes for bio-analyses and medical imaging.[1] Due to the forbidden character of the *f–f* transitions, lanthanides exhibit very low absorption coefficients, thus requiring the use of antenna molecules to indirectly excite the metal center.[2] This indirect excitation, also known as antenna effect, takes advantage of coordinated ligands that transfer energy from ligand to the metal center, resulting in lanthanide ion luminescence. In order to obtain highly luminescent molecular materials, a large number of ligands have been designed for sensitizing the luminescence of lanthanide ions.[3] Luminescence quantum yield of the complexes is one of the most important parameters for characterizing the emission performance of the materials. Generally, the luminescence quantum yield of the complexes upon excitation of the organic ligand is determined by the efficiency of the energy transfer (η_{ET}) and by the intrinsic quantum yield (Φ_{Ln}) of the lanthanide luminescence (equ. 1)

$$\Phi_{tot} = \eta_{ET}\Phi_{Ln} \quad (1)$$

According to this equation, simultaneously optimizing the two parameters is crucial in the development of systems that result in high quantum yields from lanthanide-centered emission.

In luminescence lanthanide complexes, several different excited states of chromophore can be responsible for the depopulation of the excited states of metal ions, such as singlet states,[4] triplet states,[5] intra-ligand transfer state (ILCT),[6] and metal-to-ligand charge transfer states (MLCT).[7] However, the most favored pathway is that the energy transfers from the

triplet states of ligands to the excited states of Ln(III) ions. Crosby firstly observed that the intramolecular energy transfer efficiency is a sensitive function of the relative positions of the resonance energy levels of the ions and the triplet states of the complexes.[8] After summarizing a large number of experimental data, [9] Latva gives an empirical rule that the optimal ligand-to-metal energy transfer process needs the energy difference between the excited level of Ln(III) and the lowest triplet level of the ligand is larger than 2500 cm^{-1}. Therefore, in order to make energy transfer effective, the energy-level match is one of the most important factors for designing high luminescence lanthanide complexes.

The intrinsic quantum yield (Φ_{Ln}) of the lanthanide ion luminescence expresses how well the radiative processes compete with non-radiative processes (equ. 2).

$$\Phi_{Ln} = \frac{k_r}{k_r + k_{nr}} = \frac{\tau_{obs}}{\tau_{rad}} \qquad (2)$$

Where k_r is the radiative rate constant, k_{nr} is non-radiative rate constant, τ_{obs} is the observed lifetime, τ_{rad} is the radiative lifetime. To increase intrinsic quantum yields, it is necessary to enhance the radiative transition, meanwhile suppress the non-radiative transition.

Contributions to non-radiative rate k_{nr} include back-energy transfer to the ligand and the quenching by presence of high energy oscillators, such as OH in bounded water molecules, and N–H, C–H and C=O stretching vibrations in ligands[10]. In contrast, radiative rates k_r are linked to geometric structure.[11] If there is no inversion symmetry at lanthanide ion sites, electric dipole transitions that are forbidden by odd parity become partially allowed by mixing 4f and 5d states through ligand field effects.[12] Designs of the ligands and coordination structures are directly linked to control of the ligand field. Richadson has estimated the transition intensity parameters of lanthanide complexes with the ligand field,[13] while Bennemans estimated it by using Judd-Ofelt analysis.[14] Recently, a few studies on the relationship between geometrical structures and radiative rates have been reported. Hasegawa prepared a series of Eu(III) complexes with hexafluoroacetylacetone (hfa) and various monodentate and bidentate phosphane oxide ligands.[15] With the suitably tailoring to the phosphane oxide ligand, the coordination geometries are effectively controlled. They found that the complexes with eight-coordination trigonal-dodecahedral (8-TDH) structures show higher emission quantum yields and large radiative rate constants than that observed in similar complexes with square-antiprismatic (8-SAP) structure. According to these studies, it is proposed that the radiative transition probability between 4f orbitals is enhanced by reducing the coordination structure geometrical symmetry. However, the relative researches are still scarce.

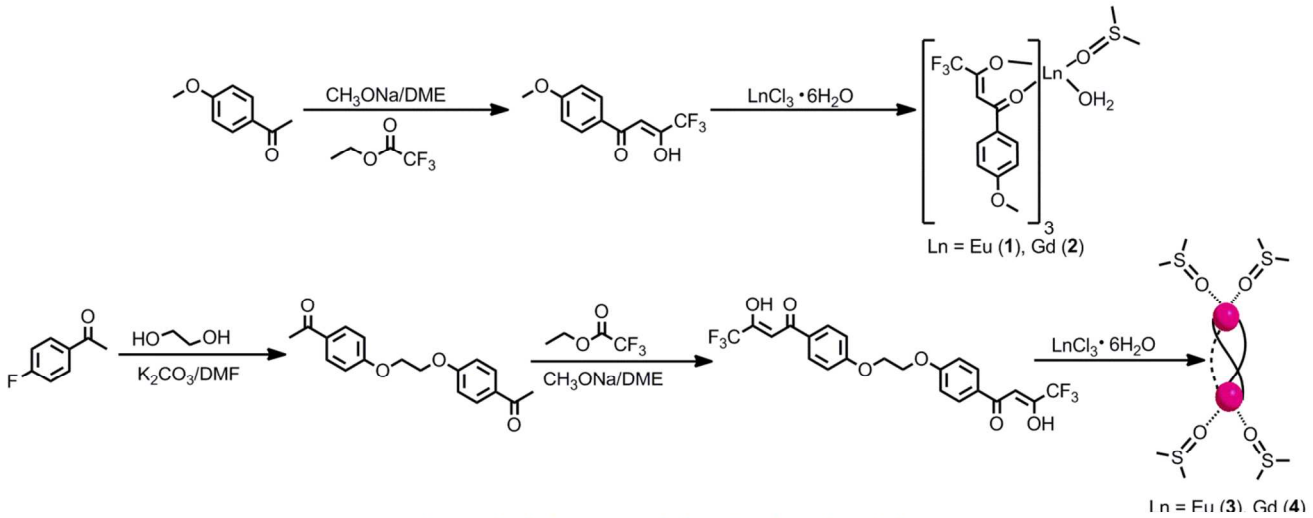

Scheme 1. Synthetic routes of the ligands and complexes **1**–**4**.

In this paper, we design and synthesize two chemical structure similar β-diketones, mono-β-diketone (p-methoxylbenzoyl)trifluoroacetone (MBTF) and bis-β-diketone 1,2-bis(4,4'-bis(4,4,4-trifluoro-1,3-dioxobutyl))phenoxyl ethane (BTPE) for the purpose of building the relationships between the structures and luminescence properties of Eu(III) complexes (Scheme 1). The bis-β-diketone (BTPE) can be looked upon as coupling of two mono-β-diketones (MBTF) at the position of methoxyl. From their chemical structures, we can conclude that the electron configurations and orbital energies in two molecules should be very similar. Thus, the two ligands should have similar photophysical properties, such as singlet states and triplet states energy levels. Therefore, the two ligands can offer a perfect model for studying the effect of the coordination structure on lanthanide ions luminescence, but not need to consider the different electron effect caused by different substituent groups. The geometrical structures of their corresponding Eu(III) complexes were characterized by single crystal X-ray analyses. The luminescence properties were characterized by their emission quantum yields, emission lifetimes, energy transfer efficiency, and their radiative and nonradiative rate constants. Based on the single crystal structures, the factors that enhanced emission quantum yields of the mono-β-diketone Eu(III) complex were elucidated in detail.

Results and discussion

Characterization of the ligands and complexes

The synthetic procedures adopted for the ligands MBTF, BTPE and their Ln(III) complexes **1**–**4** are described in Schemes 1. The ^{1}H NMR spectra of MBTF and BTPE obtained at 400 MHz in $CDCl_3$ are shown in Fig. S1 and S2 (ESI†). β-diketones generally exhibit keto-enol tautomerism. The amounts of keto- and enol form can be determined by integration of the keto and the enol resonance peaks in the ^{1}H NMR spectrum. In two spectra, the observed broad single peaks at δ 15.44 and δ 15.38 are attributed to the characteristic H^{enol} protons of MBTF and BTPE, while the methine H^{keto} protons present at δ 6.52 and δ 6.55, respectively. By integrating the areas corresponding to both species, it is found that the two ligands exist completely in the enolic form in $CDCl_3$. Two sets of double peaks observed at δ 6.98–7.04, δ 7.93–8.00 and δ 7.01–7.10 , δ 7.84–8.01 are attributed to the protons in phenylene (Hd, Hc, mono-β-diketone; Hd', Hc', bis-β-diketone). Double peaks are the results of the spin-spin coupling of the adjacent protons, and being close to the withdrawing carboxyl group makes the Hc and Hc' present at downfield. Single peaks present at δ 3.92 and δ 4.56 are attributed to methyl protons He and ethidene protons He'.

The FT–IR spectra of the complexes **1** and **2** show broad absorptions in the region of 3000–3500 cm^{-1}, thereby, indicating the presence of water molecules in the complexes. In contrast, the absence of these broad bands for **3** and **4** reveals that no water molecules present in the coordination sphere of Ln(III) ions or crystal lattice. The carbonyl stretching frequency of BTPE (1599 cm^{-1}) and MBTF (1602 cm^{-1}) have been shifted to higher wavenumbers in the complexes **1** (1618 cm^{-1}) and **3** (1616 cm^{-1}), respectively, indicating the coordination of the oxygen atoms to the lanthanide ions. This coordination is further supported by the appearance of bands in the range of 400–420 cm^{-1} due to Ln−O stretching vibrations. To examine the thermal stability and solvent contents of the complexes, thermogravimetric analyses are carried out for **1** and **3** (Fig. S3 and Fig. S4). It is clear from TG curve that complex **1** firstly undergoes a mass loss of about 1.7% (calcd 1.8%) in the first step (50−98 °C), corresponds to the loss of the coordinated water molecules, and the second step undergoes a mass loss of about 7.8% (calcd 8.0%) between 98 and 265 ℃, corresponding to the loss of the coordinated DMSO. Finally, a full decomposition is observed at ca. 290 ℃. In complex **3**, a mass loss of about 15.2% (calcd 15.0%) corresponding to the loss of two coordinated DMSO is observed in the first step (150−290 °C). The second step from 300 to 495 ℃ corresponds to the thermal decomposition of the organic ligands and finally leading to the formation of the stoichiometric amounts of Eu_2O_3.

X-ray Crystallographic Analysis

The structural analysis reveals that the complexes **1** and **3** crystallize in the triclinic space group *P*-1 and monoclinic space group *C*2/*c*, respectively. In the case of **1**, the Eu(III) is eight coordinated to two solvent molecules and three bidentate mono-β-diketonate ligands, as shown in Figure 1(a). The Eu–O distances are in the range of 2.340(5)–2.458(5) Å, the two Eu–O bonds of the coordination solvent molecules (2.433 and 2.458 Å) are longer than the six Eu–O bonds of the fluorinated β-diketonate ligands (2.340–2.417 Å).

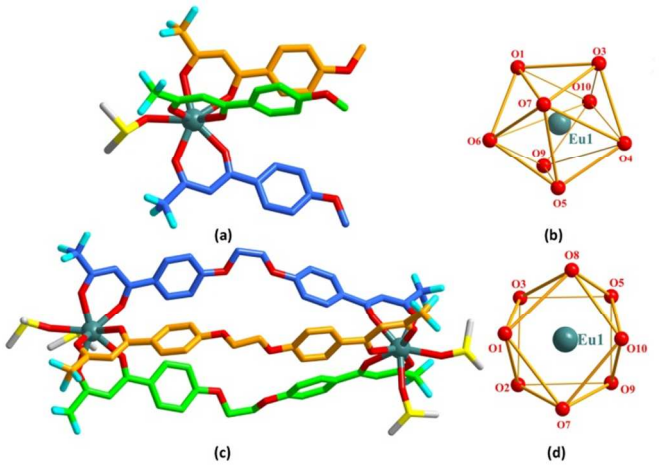

Fig. 1 Ball-and-stick representation of the crystal structures of **1** (a), **3** (c) and their coordination polyhedra (b), (d). Europium atoms are shown as cyan spheres, each ligand is represented in different colors, with oxygen atoms are colored in red.

It is interesting to observe the occurrence of C–H···O interactions in **1**, which have been recently implicated in the stabilization of transition state of catalytic transformation and the conformational preference.[16] The C–H···O interactions are found among the adjacent structural unit of **1** to give rise up to the two-dimensional layer as shown in Figure 2, among which H–bondings are observed between the terminal hydrate groups (Table S1).

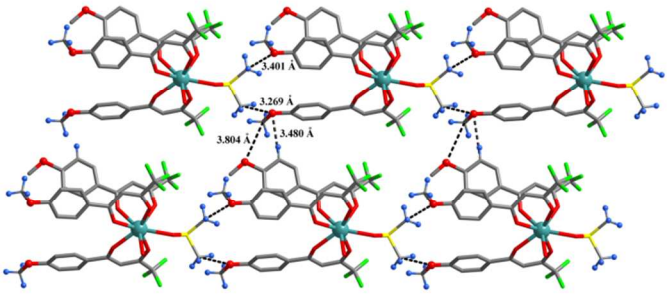

Fig. 2 Intermolecular C–H···O interactions of complex **1**

Complex **3** is a triple-stranded dinuclear helicate featured by the coordination of three bis-*β*-diketonate ligands to two crystallographically equivalent Eu(III) ions, as shown in Figure 1(c). There are four $Eu_2(BTPE)_3(DMSO)_4$ moieties per unit cell. The Eu–O distances are in the range of 2.367(5)–2.427(6) Å, which are comparable with the reported values in europium mono-*β*-diketone complexes. The Eu···Eu distance in the same helicate is 17.599 Å, which is the longest in the reported triple-

stranded bis-*β*-diketone metal complexes. The intermolecular π–π and C–H···F interactions have found their importance in the crystal engineering as for the stabilization of the molecules and the structures.[17] The structure of **3** is replete with C–H···F interactions among the adjacent helicates in the same configuration and it leads to the generation of a two-dimensional homochiral layer (Figure 3 (a)). Meanwhile, each of the six aromatic rings in the helicate of **3** forms the π–π interaction through the overlap with the adjacent aromatic ring as shown in Figure 3(b). The whole structure of **3** is stabilized through the combination of π–π and C–H···F interactions.

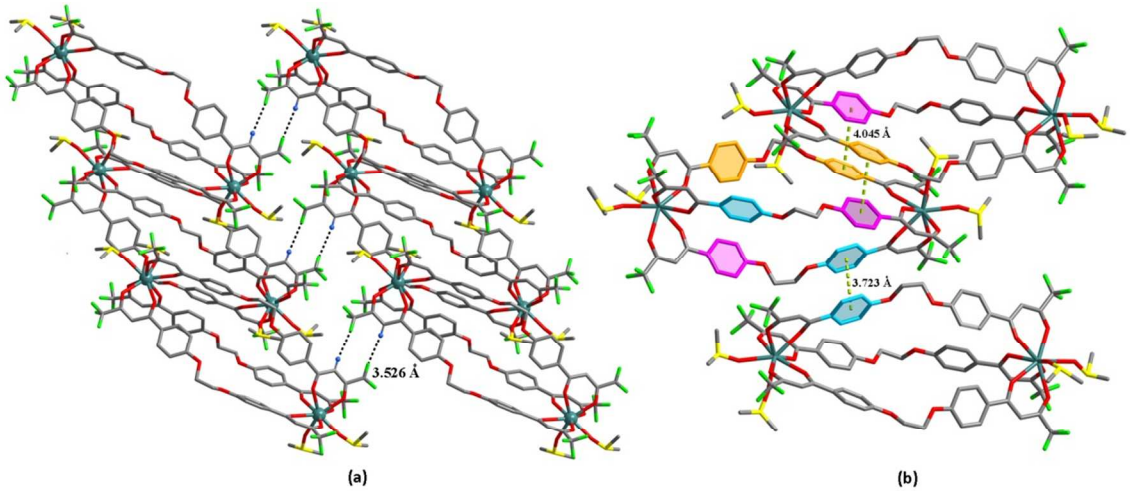

Fig. 3 Intermolecular C–H···F and π···π interactions in complex **3**

As previous reports, the emission properties of the complexes are significantly affected by the coordination environment of the Ln(III) centers. Thus, it is critical to determine the geometry of the coordition polyhedron, which is reflected by the distances and angles between the Eu and O atoms. On the basis of the crystal data, the coordination geometry of Eu(III) ions was calculated by utilizing the SHAPE 2.1 software (Table 1), and the representative coordination polyhedra are shown in Figure 1. The values given by the Shape software equals 0, corresponds to the perfect polyhedron, and the larger value indicates the more worse deviation from the ideal geometry. For complex 1, the value for the eight-coordinated triangular dodecahedron structure (8-TDH, D_{2d}, 0.828) is smaller than that for the eight-coordinated biaugmented trigonal prism structure (8-BTP, C_{2v}, 2.303), thereby the coordinated geometry of complex **1** is 8-TDH structure. In the same way, the coordinated geometry of complex **3** is classified as eight-coordianted square antiprism structure (8-SAP).

Table 1 Shape analysis of europium complexes by SHAPE 2.1 software.

Complexes	Square antiprism (D_{4d})	Triangular dodecahedron (D_{2d})	Biaugmented trigonal prism (C_{2v})
Eu(**1**)	3.071	0.828	2.303
Eu(**3**)	1.254	1.673	1.498

UV–Vis Spectra

UV–Vis absorption spectra of the ligands BTPE, MBTF and their corresponding Eu(III) complexes are shown in Figure 4. The spectral line shapes of two ligands are very similar, with the same absorption maxima at 348 nm, corresponding to singlet–singlet π–π* electronic transition of ligands. In comparison with ligands, the absorption maxima are blue-shifted about 19 nm for **1** and 24 nm for **3**.The shoulders at 364 nm in free ligands which arise from the aggregation of molecules also blue-shifted about 16 nm for two complexes, and the relative intensity to the absorptions maxima decrease significantly in complexes compared to that in ligands, indicating the reduction of aggregation extent of complexes in solution.

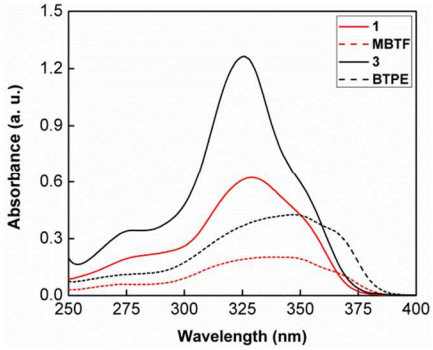

Fig. 4 UV–visible absorption spectra of MBTF, BTPE, and **1**, **3** in CH_3CN and DMSO (9:1, 1.0×10^{-5} M).

The molar absorption coefficient values of the complexes **1** and **3** are calculated as 0.63×10^5 (325 nm), 1.24×10^5 (329 nm) $L \cdot mol^{-1} \cdot cm^{-1}$, respectively. These values are about 3.0 times higher than that of the free ligands MBTF (0.20×10^5 $L \cdot mol^{-1} \cdot cm^{-1}$ at 348 nm) and BTPE (0.42×10^5 $L \cdot mol^{-1} \cdot cm^{-1}$ at 348 nm), suggesting the presence of three ligands in the corresponding complexes. The single state energy ($^1\pi\pi^*$) levels of MBTF and BTPE in complexes can be estimated by referring

to the maximum wavelengths of UV–Vis absorbance edges of their corresponding Eu(III) complexes, which have the same values at 26 881 cm^{-1} (372 nm). The same singlet energy levels and the similar spectral patterns indicate that the two ligands have very similar electron distribution and orbital energy levels.

Photoluminescent Properties of the Complexes

The emission properties of the Eu(III) complexes were investigated in the solid state at room temperature. The excitation spectra of the complexes **1** and **3** contain broad bands (240–485 nm) that correspond to the excitation of the organic chromophores (MBTF, BTPE) and several weak intra-configuration *f–f* transitions from $^7F_{0,\ 1}$ to $^5D_{0\text{-}2}$ levels. As shown in Fig. S5, the normalized excitation spectra of the two complexes almost overlap each other, except a slight intensity enhancement of the mono-*β*-diketone excitation bands at low energy region. Moreover, it is notable that the $^7F_0 \rightarrow {}^5D_2$ transitions at 464 nm show a relatively high intensity. The ratios of the intensity of these transitions to that of $S_0 \rightarrow S_1$ transition at 375 nm are 0.67 for **1** and 0.48 for **3**. It means the two complexes can emit strong red luminescence upon excitation with blue visible light at 464 nm. In addition, the excitation spectra also reveal that the energy transfer from ligands to Eu(III) center is efficient because the S_0–S_1 excitation bands are dominant over weak *f–f* transitions.

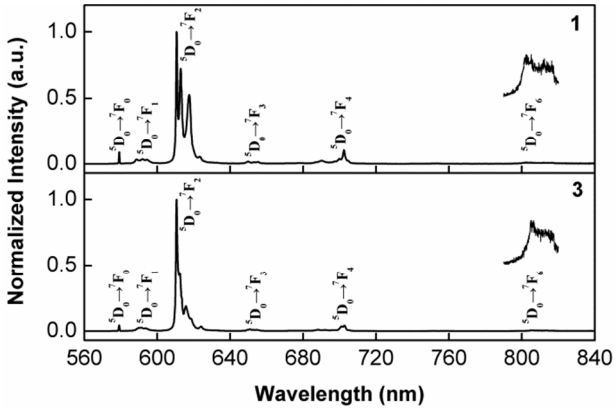

Fig. 5 Solid state emission spectra of **1** and **3** with excitation at 375 nm

The steady-state emission spectra of the europium complexes **1** and **3** in the solid state at room temperature are shown in Fig. 5. The characteristic emission bands of Eu(III) ions are observed at around 580, 592, 611, 650, 702 and 805 nm, corresponding to the $^5D_0 \rightarrow {}^7F_J$ (J = 0–4, 6) transitions, respectively. In contrast, no ligand-based emissions are observed. It demonstrates the occurrence of the effective energy transfer from the ligand to Eu(III) ions. It is well documented that the luminescent properties of lanthanide ions are sensitive to variations in the symmetry of the coordination sphere.[18] This effect can be observed from the $^5D_0 \rightarrow {}^7F_2$ transition (electric dipole), which is the strongest transition and its corresponding emission at about λ = 611 nm is very sensitive to the coordination environment. On the contrary, the $^5D_0 \rightarrow {}^7F_1$ transition is a magnetic dipole transition whose intensity is independent of the coordination environment. Therefore, the intensity ratio of the $^5D_0 \rightarrow {}^7F_2$ transition to the $^5D_0 \rightarrow {}^7F_1$ transition (I_{7F2}/I_{7F1}) reflects the nature and symmetry of the first coordination sphere. The intensity ratios of I_{7F2}/I_{7F1} are found to be 15.85 and 15.19 for complex **1** and **3**, respectively. The results reveal that the symmetry around Eu(III) ions in **1** is lower than that in **3**, which is in accordance with their coordination geometries observed from crystal structures, trigonal-dodecahedra (8-TDH) for **1** and square-antiprismtic (8-SAP) structure for **3**.

In order to investigate the relationship between structures and luminescence properties, we measured the emission quantum yields, the emission lifetimes, energy transfer efficiency, and the radiative (k_r) and nonradiative rate constants (k_{nr}) for two complexes. The parameters characterizing these properties are summarized in Table 2. The emission quantum yields of the complexes **1** and **3** were found to be 38% and 25%, respectively. The mono-β-diketonate complex **1** displays the obviously higher luminescence quantum yield than the bis-β-diketonate complex **3**. This result is contrary to that previously reported by us and others, in which the bis-β-diketonate complexes generally show higher luminescence quantum yield than the corresponding mono-*β*-diketonate complexes.[19] As shown in equation 1, the luminescence quantum yield is determined by the efficiency of the energy transfer (η_{ET}) and by the intrinsic quantum yield (Φ_{Ln}) of the lanthanide luminescence. Therefore, the higher emission quantum yield observed in **1** must originate from its relatively high intrinsic quantum yield and/or energy transfer efficiency.

The intrinsic quantum yields of europium luminescence could be estimated using the equation 2, after the calculation of the radiative lifetime (τ_{rad}) (equ. 3):

$$k_r = \frac{1}{\tau_{rad}} = A_{MD,0} n^3 \left(\frac{I_{tot}}{I_{MD}}\right) \qquad (3)$$

Where $A_{\mathrm{MD},\ 0}$ = 14.65 s^{-1} is the spontaneous emission probability of the magnetic dipole $^5D_0 \rightarrow {}^7F_1$ transition, n is the refractive index of the medium. An average index of refraction equal to 1.5 is employed. I_{tot} is the total integrated emission of the $^5D_0 \rightarrow {}^7F_J$ transitions, and I_{MD} is the integrated emission of the $^5D_0 \rightarrow {}^7F_1$ transition.

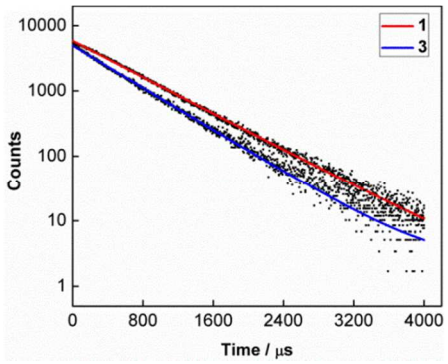

Fig. 6 Luminescence decay curves of the complex **1** and **3** monitored at 611 nm.

Table 2 Radiative (k_r) and nonradiative (k_{nr}) decay rates, observed luminescence lifetime (τ_{obs}), intrinsic quantum yield (Φ_{Ln}), sensitization efficiency (Φ_{sens}), overall quantum yield ($\Phi_{overall}$) and Judd-Ofelt intensity parameters Ω_λ (in 10^{-20} cm^2) for complexes **1** and **3** at 298K.

Complexes	I_{7F2}/I_{7F1}	Ω_2	Ω_4	Ω_6	k_r (s^{-1})	k_{nr} (s^{-1})	τ_{obs} (μs)	Φ_{Ln} (%)	Φ_{ET} (%)	$\Phi_{overall}$ (%)
1	15.85	26.5	6.4	33.5	968	637	623	60	63	38
3	15.19	25.2	5.1	24.2	895	971	536	48	52	25

The observed lifetimes (τ_{obs}) were determined by monitoring the emission decay curves within the $^5D_0 \rightarrow {}^7F_2$ transition at 611 nm. Typical decay profiles of complexes **1** and **3** are shown in Fig. 6. The two decay curves are well-reproduced by single-exponential functions, suggesting only one species exists in the excited state of the complexes. The lifetimes of the complexes **1** and **3** were found to be 623 μs and 536 μs, respectively.

With the calculated radiative lifetimes (τ_{rad}) and observed lifetimes, the intrinsic quantum yields (Φ_{Ln}) were found to be 60% and 48% for **1** and **3**. According to equation 2, the intrinsic quantum yield is the result of radiative transition competes with non-radiative transition processes. Thus, it indicates the appearance of the more dominant radiative transition to non-radiative transition in **1** than that in **3.** The radiative (k_r) and non-radiative (k_{nr}) rate constants were estimated by using the radiative lifetimes and the intrinsic quantum yields (equ. 2). We found the radiative rate constant of mononuclear complex **1** (968 s^{-1}) is higher than that in binuclear complex **3** (895 s^{-1}). Generally, reduction of the geometrical symmetry of the coordination structure leads to a larger radiative rate constant.[14,15] Thus, we propose the larger radiative rate constant in **1** should arise from its lower symmetrical 8-TDH structure compared with 8-SAP coordinate geometry in **3**. In contrast, the non-radiative rate constants were found to be 637 s^{-1} and 971 s^{-1} for complexes **1** and **3**, respectively. It is well known that the quenching of lanthanide excitation state by non-radiative transition is mainly caused by the matrix vibrations, especially by the bounded solvent molecules. The O–H oscillator is considered to be the most effective quencher. Other oscillators are less efficient, but clear evidence for the quenching effect of high harmonics of C–H and C=O stretching vibrations was provided. In two complexes, the coordinated solvent molecules are different. Mononuclear Eu(III) ion is coordinated by a water and a DMSO molecules in its first coordination sphere, whereas binuclear Eu(III) ion by two DMSO molecules. Therefore, the contributions of solvents to quench Eu(III) ions excited state should be greater in **1** than that in **3**, due to the presence of higher energy O–H vibration to metal center (Eu–O, 2.257 Å). However, the opposite result is observed that the complex **3** shows faster non-radiative rates. Therefore there must exist other more effective deactivation pathways to quench the luminescence of Eu(III) ions in **3**. Due to the less efficient quenching effect of the C–H stretching vibrations of ligands and their similar distance to the metal centers, we thought the contributions of C–H oscillators to nonradiative transition should be about the same and limited.

Back-energy transfer from lanthanide excited states to the singlet states and/or triplet states of ligands is also an effective way for quenching lanthanide ions luminescence.[20] According to Latva's empirical rule, if the energy gap $\Delta E(^3\pi\pi^* - {}^5D_0) < 2500$ cm^{-1}, back energy transfer from the Eu(III) excited state to the triplet state of ligands will become more efficient. The triplet energy levels of two ligands are estimated by referring to their lower emission edges of the corresponding phosphorescence spectra. On account of the difficulty in observing the phosphorescence of the ligands, the emission spectra of their Gd(III) complexes $[Gd(MBTF)_3(DMSO)(H_2O)]$ (**2**) and $[Gd_2(BTPE)_3(DMSO)_4]$ (**4**) at 77 K were used to estimate the triplet state energy levels. Because the lowest excited energy level of Gd^{3+} ion ($^6P_{7/2}$) is too high to accept energy from the ligand, the triplet state energy level of the ligand is not significantly affected by the Gd^{3+} ion. As shown in Fig. S6, the phosphorescence spectra of two complexes **2** and **4** are very similar with about the same lower emission edges at 21 053 cm^{-1} (475 nm). The energy gap $\Delta E(^3\pi\pi^* - {}^5D_0)$ is 3753 cm^{-1}. Based on this result, the energy transfer from triplet state to excited state of Eu(III) ions in two complexes should be efficient, and the back energy transfer rates should also be the same. However, according to a detail analysis to the crystal structures, we can observe that there are a large number of intermolecular π–π interactions in **3** (Figure 3 (b)). In contrast, there are no π–π interactions observed in mononuclear complex **1**. It is well known that the π–π interactions will obviously lower the excited state energy levels of ligands. Therefore, the true triplet energy level of the bis-*β*-diketone would be lower than this value. This reduction of the energy gap subsequently leads to the faster back energy transfer rates, and larger nonradiative rate constant. In addition, it is the reason that the energy transfer efficiency for **3** (52%) is lower than that observed in **1**(63%). According to above discussions, the higher luminescence quantum yield of mono-β-diketonate complex can be attributed to its lower site symmetry around the Eu(III) ion, lower non-radiative rate constant and higher energy transfer efficiency from ligand to metal ion.

Judd-Ofelt Analysis

The Judd–Ofelt theory is a useful tool for estimating the probability of the forced electric dipole transitions of the rare-earth ions in various environments. The intensity parameters Ω_λ (λ = 2, 4, 6), related to the interaction of ligand fields parameters, are particularly sensitive towards symmetry and sequence of ligand fields.[21] It can be determined experimentally after giving the probability of electric dipole transition (A_{ed}) according to equ. 4.

$$A_{ed} = A\left[f^N\psi_J; f^N\psi'_{J'}\right] = \frac{64\pi^4 e^2}{3h}\frac{v^3}{(2J+1)}\frac{n(n^2+2)^2}{9}D_{ed} =$$

$$\frac{64\pi^4 e^2}{3h}\frac{v^3}{(2J+1)}\frac{n(n^2+2)^2}{9}\sum_{\lambda=2,4,6}\Omega_\lambda\left|\langle f^N\psi_J\|U^{(\lambda)}\|f^N\psi'_{J'}\rangle\right|^2 \quad (4)$$

where n is the refractive index of the medium, h the Planck's constant, e the electron charge in electro static unit, υ the average energy of the transition in cm^{-1}, and (2J + 1) the degeneracy of the $^5D_0$. $|\langle f^N\psi_J \| U^{(\lambda)} \| f^N\psi_{J'}\rangle|^2$ are the squared reduced matrix elements whose values vary only slightly in different matrix for a given trivalent lanthanide ion, and therefore it is often used as a constant. The transition of $^5D_0 \rightarrow {}^7F_1$ is a magnetic dipole transition which is independent of the ion surroundings and can be used as a reference. The spontaneous emission probability of magnetic dipole transition (A_{md}) can be estimated using eqn. 5.

$$A_{\mathrm{md}} = \frac{64\pi^4}{3h}\frac{v^3}{(2J+1)}n^3 D_{md} \quad (5)$$

Where D_{md} is the strength of magnetic dipole transition whose value is 9.6×10^{-42} esu^2 cm^2. Therefore, the probability of electric dipole transition (A_{ed}) can be determined from the ratios of integrating emission intensities of $^5D_0 \rightarrow {}^7F_{2,4,6}$ transitions to the intensity of $^5D_0 \rightarrow {}^7F_1$ transition as follows:

$$A_J = \frac{\int I_J(v)\,dv}{\int I_{md}(v)\,dv}A_{md} \quad (6)$$

According to equ.4–6, the Judd-Ofelt parameters have been determined and the values are summarized in Table 2. Among the three J–O parameters, Ω_2 parameter depend on the local environment around the Eu(III) site, whereas Ω_4 and Ω_6 are related to the bulk properties of the host material in which the ions are situated.[22] The Ω_2 values of complex **1** and **3** are found to be 26.5×10^{-20} cm^2 and 25.2×10^{-20} cm^2, respectively. The higher Ω_2 value observed in **1** indicates that there exists lower symmetry than that in **3**, in agreement with the coordination geometries of the Eu(III) ions observed in structures. To get faster Eu(III) radiative rates, asymmetrical Eu(III) complexes with larger Ω_2 need to be designed. The Ω_4 and Ω_6 values of complexes **1** and **3** are found to be 6.4×10^{-20} cm^2, 5.1×10^{-20} cm^2 and 33.5×10^{-20} cm^2, 24.2×10^{-20} cm^2, respectively. It means that the steric effects are more significant in complex **1**, which may be the reason why only one bulk DMSO molecule can presents in Eu(III) ion first coordination sphere, whereas the appearance of two bulk DMSO molecules in **3**.

Conclusion

In summary, we employed two chemical structures similar mono-*β*-diketone and bis-*β*-diketone synthesizing two different coordination geometries mononuclear and binuclear europium complexes. The complexes exhibit characteristic luminescence properties that depend on their coordination structure. Compared to the binuclear complex **3** with 8-SAP structure, the mononuclear complex **1** shows faster radiative rate due to its lower symmetrical 8-TDH structure. Whereas, the complex **3** display the faster nonradiative rate and lower energy transfer efficiency due to the enhanced back-energy transfer probability caused by the intermolecular π–π interactions. Therefore, the higher luminescence quantum yield of complex **1** mainly benefits from its lower symmetrical coordination structure and the absence of the intra- or inter-molecular π–π interactions. In this paper, though the bis-β-diketonate complex did not display the better luminescent performance, bis-β-diketones still have advantages on designing the high luminescence lanthanide complex, that is the symmetry around Ln(III) ion can be easily controlled by selecting different spacers between the two β-diketones units.

Experimental

Materials and instruments

The commercially available chemicals were analytical reagent grade and used without further purification. $LnCl_3 \cdot 6H_2O$ was prepared according to the literature by dissolving 99.99% oxide in a slight excess of hydrochloric acid. The solution was evaporated and the precipitate was collected from water.

Elemental analyses were performed on an Elementar Vario EL cube analyzer. FT-IR spectra were obtained on a Perkin-Elmer Spectrum One spectrophotometer by using KBr disks in the range of 4000–370 cm^{-1}. UV spectra were recorded on a Perkin-Elmer Lambda 25 spectrometer. Thermal analyses were conducted on a Perkin-Elmer STA 6000 with a heating rate of 10 ºC·min^{-1} in a temperature range from 30 ºC to 800 ºC. The ^1H NMR spectra were recorded on a Bruker Avance III 400 MHz spectrometer in $CDCl_3$ solution. Electron ionization (EI) and Electrospray time-of-flight (ESI-TOF) mass spectra were recorded on Agilent 5973N and Bruker maXis mass spectrometers, respectively. Crystal data of the complexes were collected on a Xcalibur, Eos, Gemini diffractometer with Mo Kα radiation (λ = 0.71073 Å). All data were collected at a temperature of 23 ± 2 ºC.The structures were solved by the direct methods and refined on F^2 by full-matrix least-squares using the SHELXTL-97 program. The Ln^{3+} ions were easily located and then non-hydrogen atoms (C, O and F) were placed from the subsequent Fourier-difference maps. All non-hydrogen atoms were refined anistropically. The data collection and refinements were given in Table S2. Excitation and emission spectra were measured with an Edinburgh FLS 920 fluorescence spectrophotometer equipped with a red-sensitive photomultiplier detector (Hamamatsu R928). Luminescence lifetimes were recorded on a single photon counting spectrometer from Edinburgh Instrument (FLS 920) with a microsecond pulse lamp as the excitation sources. The data were analysed by software supplied by Edinburgh Instruments. The quantum yields for the complexes were determined at room temperature through an absolute method using an Edinburgh instruments integrating sphere coupled to the modular Edinburgh FLS 920 fluorescence spectrophotometer. The values reported are the average of three independent determinations for each sample. The absolute quantum yield was calculated using the following expression:

$$\Phi = \frac{\int L_{emisson}}{\int E_{reference} - \int E_{sample}}$$

Where $L_{emission}$ is the emission spectrum of the sample, collected using the sphere, E_{sample} is the spectrum of the incidence light used to excite the sample, collected using the sphere, $E_{reference}$ is the spectrum of the light used for excitation with only the reference in the sphere. The method is accurate within 10%.

Synthesis of 1,2-bis(4,4'-bis(acetyl phenoxy))ethane. The reaction (Scheme 1) was conducted in a 500 mL three-necked round–bottom flask that was equipped with a mechanical stirrer, a nitrogen inlet and a condenser. A mixture of DMF (150 mL), potassium carbonate anhydrous (4.50 g, 0.030 mol), 4'-fluoroacetophenone (22.30 g, 0.16 mol) were added in the reaction vessel and heated to reflux under nitrogen with stirring. Then a DMF solution (50 mL) of ethylene glycol (2.0 g, 0.030 mol) was added over a period of 1 h. The solution was kept to reflux for another 12 h to ensure the completion of the reaction, and then it was cooled and filtered to remove the salt. The solution was poured into 500 mL distilled water to precipitate the product. The precipitate was collected by filtration and washed with water three times, and then it was washed with ethanol three times. The solid was dried by drawing air through the filter cake for 1 h. Crude product was purified by crystallization from acetone to give white crystals (6.72 g, 70%). Anal. Calc. for $C_{18}H_{18}O_4$ (298.33): C, 72.47; H, 6.08; O, 21.45. Found: C, 72.40; H, 6.17; O, 21.36. IR (KBr, cm^{-1}): 3332, 1676, 1596, 1253, 1174, 819. ^1H NMR ($CDCl_3$, 400 MHz): 7.93–8.01 (d, 4H), 6.98–7.05 (d, 4H), 4.44 (s, 4H), 2.58 (s, 6H).

Synthesis of 1,2-bis(4,4'-bis(4,4,4-trifluoro-1,3-dioxobutyl))phenoxy ethane (BTPE). A mixture of sodium methoxide (5.41 g, 0.1 mol) and ethyl trifluoroacetate (14.32 g, 0.10 mmol) in 40 mL dry DME (ethylene glycol dimethyl ether) was stirred for 10 min, followed by the addition of 1,2-bis(4,4'-bis(acetyl phenoxy))ethane (10.01 g, 0.034 mol). Then, it was further stirred at room temperature for 24 h (Scheme 1). The resulting mixture was poured into 100 mL ice-water and acidified to pH = 2–3 using hydrochloric acid (2 M), and the resulting white precipitate was filtered and dried in vacuum. Recrystallization from acetone gave white flake crystals (11.20 g, 69%). Anal. Calc. for $C_{22}H_{16}F_6O_6$ (490.35): C, 53.89; H, 3.29; O, 19.58. Found: C, 53.95; H, 3.18; O, 19.49. IR (KBr, cm^{-1}): 3650, 1599, 1509, 1456, 1250, 1176, 798. ^1H NMR ($CDCl_3$, 400 MHz): 15.38 (s, 2H, Ha'), 7.84–8.01 (d, 4H, Hc'), 7.01–7.10 (d, 4H, Hd'), 6.55 (s, 2H, Hb'), 4.45 (s, 4H, He'). ESI–MS m/z 491.47 $[BTPE + H]^+$.

Synthesis of (p-methoxylbenzoyl)trifluoroacetone (MBTF). A mixture of sodium methoxide (7.20 g, 0.13 mol) and ethyl trifluoroacetate (18.92 g, 0.13 mol) in 40 mL dry DME (ethylene glycol dimethyl ether) was stirred for 10 min, followed by the addition of p-methoxyacetophenone (10.02 g, 0.07 mol). Then, it was further stirred at room temperature for 24 h (Scheme 1). The resulting mixture was poured into 100 mL ice-water and acidified to pH = 2–3 using hydrochloric acid (2 M). The resulting white precipitate was filtered and dried in vacuum. Recrystallization from acetone gave white flake crystals (8.55 g, 52%). Anal. Calc. for $C_{11}H_9F_3O_3$ (246.18): C, 53.67; H, 3.68; O, 19.50. Found: C, 53.60; H, 3.74; O, 19.58. IR (KBr, cm^{-1}): 3118, 1602, 1509, 1271, 1169, 1110, 793. ^1H NMR ($CDCl_3$, 400 MHz): 15.41 (s, 1H, Ha), 7.95–7.99 (d, 2H, Hc), 6.99–7.05 (d, 2H, Hd), 6.53 (s, 1H, Hb), 3.92 (s, 3H, He). ESI–MS m/z 269.31 $[MBTF + Na]^+$.

Synthesis of Ln(MBTF)$_3$(DMSO)(H$_2$O) [Ln = Eu, Gd]. MBTF (1.03 g, 4.06 mmol) and triethylamine (0.41 g, 4.06 mmol) were dissolved in hot MeOH (20 mL). To this solution cooled to room temperature, $LnCl_3 \cdot 6H_2O$ (1.35 mmol) in MeOH (10 mL) was added dropwise and it was further stirred 24 h (Scheme 1). The precipitate formed after the addition of water was filtered and dried in vacuum. Recrystallization from DMSO and $CHCl_3$ gave white needle crystals.

*Eu(MBTF)$_3$(DMSO)(H$_2$O) (**1**)*. Yield: 83%. Anal. Calc. for $C_{35}H_{32}F_9O_{11}SEu$ (983.64): C, 42.74; H, 3.28; O, 17.89; S 3.26. Found: C, 42.67; H, 3.35; O, 17.78; S 3.21. IR (KBr, cm^{-1}): 3335, 1616, 1505, 1292, 1177, 1024, 791. ESI–MS *m/z* 911.24 $[Eu(MBTF)_3 + Na]^+$.

*Gd(MBTF)$_3$(DMSO)(H$_2$O) (**2**)*. Yield: 82%. Anal. Calc. for $C_{35}H_{32}F_9O_{11}SGd$ (988.92): C, 42.51; H, 3.26; O, 17.80; S 3.24. Found: C, 42.57; H, 3.33; O, 17.75; S 3.20. IR (KBr, cm^{-1}): 3421, 1615, 1504, 1291, 1180, 1124, 790. ESI–MS *m/z* 916.12 $[Gd(MBTF)_3 + Na]^+$.

Synthesis of Ln$_2$(BTPE)$_3$(DMSO)$_4$ [Ln = Eu, Gd]. BTPE (0.50 g, 1.02 mmol) and triethylamine (0.21 g, 2.04 mmol) were dissolved in hot MeOH (20 mL). To this solution cooled to room temperature, $LnCl_3 \cdot 6H_2O$ (0.68 mmol) in MeOH (10 mL) was added dropwise and it was further stirred 24 h (Scheme 1). The precipitate formed after the addition of water was filtered and dried in vacuum. Recrystallization from DMSO and $CHCl_3$ gave white needle crystals.

*Eu$_2$(BTPE)$_3$(DMSO)$_4$ (**3**)*. Yield: 81%. Anal. Calc. for $C_{74}H_{66}F_{18}O_{22}S_4Eu_2$ (2081.46): C, 42.70; H, 3.20; O, 16.91; S 6.16. Found: C, 42.75; H, 3.32; O, 16.88; S 6.24. IR (KBr, cm^{-1}): 2931, 1602, 1503, 1294, 1253, 1178, 1134, 788. ESI–MS *m/z* 1791.94 $[Eu_2(BTPE)_3 + Na]^+$.

*Gd$_2$(BTPE)$_3$(DMSO)$_4$ (**4**)*. Yield: 80%. Anal. Calc. for $C_{74}H_{66}F_{18}O_{22}S_4Gd_2$ (2092.03): C, 42.48; H, 3.18; O, 16.83; S 6.13. Found: C, 42.39; H, 3.25; O, 16.77; S 6.20. IR (KBr, cm^{-1}): 2930, 1601, 1504, 1296, 1247, 1177, 1142, 792. ESI–MS *m/z* 1802.51 $[Gd_2(BTPE)_3 + Na]^+$.

Acknowledgements

This work is financially supported by the National Natural Science Foundation of China (Nos. 51302068 & 21272061 & 51472076).

Notes and references

Key Laboratory of Functional Inorganic Material Chemistry (Heilongjiang University), Ministry of Education, School of Chemistry and Materials Science, Heilongjiang University, Harbin 150080, PR China. Fax: 86-451-86608042 E-mail: lhf4612@163.com; yanpf@vip.sina.com

Electronic Supplementary Information (ESI) available: ^{1}H NMR spectra of ligands, TG patterns, CCDC reference numbers 1052336-1052337 for **1** and **3**. Phosphorescence spectra of the complexes **2** and **4** at 77 K, and solid state excitation spectra of **1** and **3**. See DOI:10.1039/b000000x/

1 (a) S. V. Eliseeva and J.-C. G. Bünzli, *Chem. Soc. Rev.*, 2010, **39**, 189–227; (b) J.-C. G. Bünzli, *Chem. Rev.*, 2010, **110**, 2729–2755; (c) J. Kido and Y. Okamoto, *Chem. Rev.*, 2002, **102**, 2357–2368; (d) L. F. Smith, B. A. Blight, H.-J. Park and S. Wang, *Inorg. Chem.*, 2014, **53**, 8036−8044; (e) G. H. Dennison, M. R. Sambrook and M. R. Johnston, *Chem. Commun.*, 2014, **50**, 195–197; (f) X. H. Wang, H. J. Chang, J. Xie, B. Z. Zhao, B. Liu, S. L. Xua, W. B. Pei, N. Ren, L. Huang and W. Huang, *Coord. Chem. Rev.*, 2014, **273**, 201–212; (g) L. D. Carlos, R. A. S. Ferreira, V. de Zea Bermudez, B. Julián-López and P. Escribano, *Chem. Soc. Rev.*, 2011, **40**, 536–549; (h) J. Feng and H. J. Zhang, *Chem. Soc. Rev*., 2013, **42**, 387−410; (i) J.-C. G. Bünzli and S. V. Eliseeva, *Chem. Sci.*, 2013, **4**, 1939–1949; (j) M. C. Heffern, L. M. Matosziuk and T. J. Meade, *Chem. Rev.*, 2014, **114**, 4496−4539.

2 C. Piguet and J.-C. G. Bünzli, *Chem. Soc. Rev*., 2005, **34**, 1048–1077.

3 (a) J. P. Byrne, J. A. Kitchen, J. E. O'Brien, R. D. Peacock and T. Gunnlaugsson, *Inorg. Chem.*, 2015, **54**, 1426−1439; (b) D. B. A. Raj, B. Francis, M. L. P. Reddy, R. R. Butorac, V. M. Lynch and A. H. Cowley, *Inorg. Chem.*, 2010, **49**, 9055–9063; (c) J. Shi, Y. J. Hou, W. Y. Chu, X. H. Shi, H. Q. Gu, B. L. Wang and Z. Z. Sun, *Inorg. Chem.*, 2013, **52**, 5013−5022; (d) D. B. A. Raj, S. Biju and M. L. P. Reddy, *Inorg. Chem.*, 2008, **47**, 8091–8100; (e) C. Freund, W. Porzio, U. Giovanella, F. Vignali, M. Pasini and S. Destri, *Inorg. Chem.*, 2011, **50**, 5417–5429.

4 (a) C. Yang, L. M. Fu, Y. Wang, J. P. Zhang, W. T. Wong, X. C. Ai, Y. F. Qiao, B. S. Zou and L. L. Gui, *Angew. Chem. Int. Ed.*, 2004, **43**, 5010–5013; (b) J. Andres and A.-S. Chauvin, *Phys. Chem. Chem. Phys.*, 2013, **15**, 15981–15994.

5 M. B. S. Botelho, M. D. Gálvez-López, L. De Cola, R. Q. Albuquerque and A. S. S. de Camargo, *Eur. J. Inorg. Chem*., 2013, 5064–5070.

6 (a) A. D'Aléo, F. Pointillart, L. Ouahab, C. Andraud and O. Maury, *Coord. Chem. Rev.*, 2012, **256**, 1604–1620; (b) F. Pointillart, A. Bourdolle, T. Cauchy, O. Maury, Y. L. Gal, S. Golhen, O. Cador and L. Ouahab, *Inorg. Chem*., 2012, **51**, 978–984; (c) F. Pointillart, T. Cauchy, O. Maury, Y. L. Gal, S. Golhen, O. Cador and L. Ouahab, *Chem. Eur. J.*, 2010, **16**, 11926–11941.

7 (a) M. D. Ward, *Coord. Chem. Rev.*, 2010, **254**, 2634–2642; (b) L. J. Xu, G. T. Xu and Z. N. Chen, *Coord. Chem. Rev.*, 2014, **273**, 47–62; (c) Q. H. Wei, Y. F. Lei, W. R. Xu, J. M. Xie and G. N. Chen, *Dalton Trans.*, 2012, **41**, 11219–11225; (d) L. N. Li, S. Q. Zhang, L. J. Xu, Z. N. Chen and J. H. Luo, *J. Mater. Chem. C.*, 2014, **2**, 1698–1703; (e) D. Sykes, A. J. Cankut, N. M. Ali, A. Stephenson, S. J. P. Spall, S. C. Parker, J. A. Weinstein and M. D. Ward, *Dalton Trans.*, 2014, **43**, 6414–6428.

8 G. A. Crosby, R. M. Alire and R. E. Whan, *J. Chem. Phys*., 1961, **34**, 743–748.

9 M. Latva, H. Takalo, V.-M. Mukkala, C. Matachescu, J. C. Rodriguez-Ubis and J. Kankare, *J. Lumin*., 1997, **75**, 149–169.

10 (a) Y. Haas and G. Stein, *J. Phys. Chem.*, 1971, **75**, 3677–3681; (b) A. Beeby, I. M. Clarkson, R. S. Dickins, S. Faulkner, D. Parker, L. Royle, A. S. de Sousa, J. A. G. Williams and M. Woods, *J. Chem. Soc., Perkin Trans. 2.*, 1999, 493–504.

11 (a) Z. Ahmed and K. Iftikhar, *J. Phys. Chem. A*, 2013, **117**, 11183−11201; (b) L. J. Daumann, D. S. Tatum, B. E. R. Snyder, C. Ni, G.-L. Law, E. I. Solomon and K. N. Raymond, *J. Am. Chem. Soc*., 2015, **137**, 2816−2819.

12 C. Görller-Walrand and K. Binnemans, *Handbook on the Physics and Chemistry of Rare Earths*, Elsevier: Amsterdam, 1998, **25**, 101–252.

13 A. F. Kirby, F. S. Richardson, *J. Phys. Chem.*, 1983, **87**, 2544–2556.

14 K. Binnemans, R. V. Deun, C. Görller-Walrand, S. R. Collinson, F. Martin, D. W. Bruce and C. Wickleder, *Phys. Chem. Chem. Phys.*, 2000, **2**, 3753–3757.

15 (a) Y. Hasegawa, T. Ohkubo, T. Nakanishi, A. Kobayashi, M. Kato, T. Seki, H. Ito and K. Fushimi, *Eur. J. Inorg. Chem*., 2013, **34**, 5911–5918; (b) K. Miyata, T. Nakagawa, R. Kawakami, Y. Kita, K. Sugimoto, T. Nakashima, T. Harada, T. Kawai and Y. Hasegawa, *Chem. Eur. J.*, 2011, **17**, 521–528; (c) K. Nakamura, Y. Hasegawa, H. Kawai, N. Yasuda, N. Kanehisa, Y. Kai, T. Nagamura, S. Yanagida and Y. Wada, *J. Phys. Chem. A.*, 2007, **111**, 3029–3037; (d) Y. Hasegawa, S. Tsuruoka, T. Yoshida, H. Kawai and T. Kawai, *J. Phys. Chem. A.*, 2008, **112**, 803–807; (e) K. Miyata, Y. Hasegawa, Y. Kuramochi, T. Nakagawa, T. Yokoo and T. Kawai, *Eur. J. Inorg. Chem*., 2009, **32**, 4777–4785.

16 (a) G. R. Desiraju, *Chem. Commun*., 2005, 2995–3001; (b) C. R. Jones, P. K. Baruah, A. L. Thompson, S. Scheiner and M. D. Smith, *J. Am. Chem. Soc.*, 2012, **134**, 12064−12071.

17 (a) Y. H. Wan, L. P. Zhang, L. P. Jin, S. Gao and S. Z. Lu, *Inorg. Chem*., 2003, **42**, 4985–4994; (b) Z. H. Sun and L. W. McLaughlin, *J. Am. Chem. Soc*., 2007, **129**, 12531–12536.

18 (a) N. S. Baek, Y. H. Kim and D. H. Lee, *Bull. Kor. Chem. Soc*., 2009, **30,** 1553–1558; (b) E. Deiters, B. Song, A.-S. Chauvin, C. D. B. Vandevyver and J.-C. G. Bünzli, *New J. Chem.*, 2008, **32**, 1140–1152; (c) D. Ananias, F. A. Almeida Paz, D. S. Yufit, L. D. Carlos and J. Rocha, *J. Am. Chem. Soc.*, 2015, **137**, 3051–3058; (d) I. P. Roof, M. D. Smith, S. Park and H.-C. zur Loye, *J. Am. Chem. Soc*., 2009, **131**, 4202–4203.

19 (a) H. F. Li, P. F. Yan, P. Chen, Y. Wang, H. Xu and G. M. Li, *Dalton Trans*., 2012, **41**, 900–907; (b) A. P. Bassett, S. W. Magennis, P. B. Glover, D. J. Lewis, N. Spencer, S. Parsons, R. M. Williams, L. D. Cola and Z. Pikramenou, *J. Am. Chem. Soc*., 2004, **126**, 9413–9424; (c) H. F. Li, G. M. Li, P. Chen, W. B. Sun and P. F. Yan, *Spectrochim. Acta Part A.*, 2012, **97**, 197–201; (d) J. Q. Leng, H. F. Li, P. Chen, W. B. Sun, T. Gao and P. F. Yan, *Dalton Trans*., 2014, **43**, 12228–12235.

20 M. H. V. Werts, R. T. F. Jukes and J. W. Verhoeven, *Phys. Chem. Chem. Phys*., 2002, **4**, 1542–1548.

21 M. P. Hehlen, M. G. Brik and K. W. Krämer, *J. Lumin*., 2013, **136**, 221–239.

22 L. D. Carlos, Y. Messaddeq, H. F. Brito, R. A. S Ferreira, V. de Zea Bermudez and S. J. L. Ribeiro, *Adv. Mater.*, 2000, **12**, 594–598.